Instabilities and amplification of counterpropagating waves in a Kerr nonlinear medium

C. T. Law and A. E. Kaplan

Department of Electrical and Computer Engineering, Johns Hopkins University, Baltimore, Maryland 21218

Received December 8, 1989; accepted June 14, 1990

We show that two linearly polarized counterpropagating waves in a Kerr nonlinear medium with linear dispersion can exhibit amplification and multimode temporal instability, which are attributed to the combined effect of nonlinear index grating and linear dispersion. At the onset of the instability, some modes become unstable, and the ensuing oscillations are periodically modulated; as pumping further increases, the motion becomes chaotic. With the pumping below the threshold, the system exhibits large amplification. In an optical fiber, appreciable gain is anticipated even with pumping much below the threshold.

1. INTRODUCTION

The cross interaction of two counterpropagating laser beams[1–6] in a third-order nonlinear material is a conceptually simple and fundamental process in nonlinear optics. The steady states of this interaction have been shown to exhibit various interesting and complicated features including hysteresis and optical bistability,[1] nonlinear eigenpolarizations that remain intact as the beams propagate[2] (which can be spatially stable or unstable[3,4]), and multivalued solutions with both the hysteretic and isolated (nonhysteretic) solutions.[3] The possibility of chaotic *spatial* behavior[5] has also been indicated.

The temporal behavior of counterpropagating nonlinear waves is even more complex and is of great significance to such systems as lasers, optical gyroscopes, and various nonliner optical bistable devices. Earlier theoretical investigations demonstrated the existence of *temporal* instability and chaos under various extensions of this system, in particular, for a nonlinear medium having finite relaxation time.[6] While the result in Ref. 6 was obtained for the simplest (spatially stable) eigenpolarization with two counterpropagating beams having linear polarizations parallel to each other, temporal instability of the beam polarizations was shown in Ref. 4 within the same system in the presence of relaxation for various nonlinear eigenpolarizations[2] (as well as in the case of instantaneous nonlinearity for a spatially unstable eigenpolarization). However, the relaxation of the nonlinear refractive index may not be the most likely mechanism of instability of beam intensity in most of the nonlinear systems, since it imposes too stringent requirements on relaxation time.

Recently we showed[7] that another physical factor, namely, regular linear dispersion (i.e., frequency dependence of the refractive index), can be a natural and universal agent for amplification of perturbations and temporal instability in the counterpropagating nonlinear waves. In this paper we present a detailed study of the effect and also explore its possible use for large broadband amplification that may exist in the system if the pumping is below the threshold of instability. It is well known that linear dispersion can give rise to nonlinear optical effects such as spatial instability of a single plane wave,[8] formation of solitons in nonlinear fibers,[9] and amplification of copropagating waves.[10] This suggests that linear dispersion, in combination with nonlinear processes, can dramatically change the dynamical behavior of a system. Surprisingly, this factor has not been discussed in applications to the problem under consideration.

In order to demonstrate the instability effect, we investigate the simplest spatially stable eigenpolarization,[2,3] whereby the two waves are linearly polarized with electrical fields parallel to each other. (Spatial stability of the eigenpolarization is essential, since spatially unstable polarization arrangements may result in temporal instability even if no other mechanism is present.[11]) We consider field envelopes as time dependent and use nonlinear Maxwell's equations (Section 2) with their linear parts, including the lowest-order term describing frequency dispersion in the form, which is conventionally used in the theory of instability and solitons in single-wave propagation.[8,9] With linear stability analysis (Section 3), we obtain an expression for instability threshold (Section 4) as a function of linear dispersion, nonlinearity, and pumping intensity and show that, when the pumping intensity exceeds a certain threshold, the system becomes unstable. We discuss the changes in behavior of the system as the pumping intensity increases, in particular, periodic oscillations of the envelope and chaos (Section 5). We consider further the case when the pumping intensity is below the threshold (Section 6); under this condition, the system exhibits large (theoretically unlimited) small-signal gain and broadband amplification, which is of particular interest for optical fiber, for which a considerable gain can be attained at low pumping intensity.

2. WAVE EQUATIONS FOR COUNTERPROPAGATING BEAMS

For the configuration shown in Fig. 1, the total complex electric field of the two counterpropagating plane waves in the Kerr nonlinear medium is represented as

0740-3224/91/010058-10$05.00

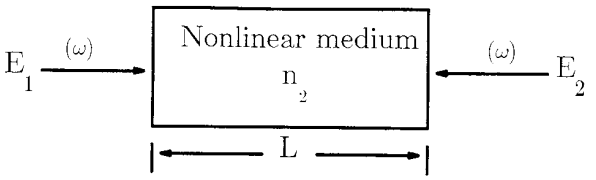

Fig. 1. Counterpropagating waves in a Kerr nonlinear medium.

$$\mathbf{E} = [E_1(z,t)\exp(ikz) + E_2(z,t)\exp(-ikz)]\exp(-i\omega t)\hat{e}_x, \tag{1}$$

where $E_1(z,t)$ and $E_2(z,t)$ are the slowly varying envelopes of forward $(+z)$ and backward $(-z)$ propagating waves, respectively. The dynamics of these envelopes is governed by two coupled nonlinear Schrödinger equations[7]:

$$i\left[(-1)^{j+1}\frac{\partial E_j}{\partial z} + \frac{1}{v_g}\frac{\partial E_j}{\partial t}\right] - \frac{\mu}{2}\frac{\partial^2 E_j}{\partial t^2} = -\beta(2I_{3-j} + I_j)E_j \qquad j = 1,2, \tag{2}$$

where $I_j = |E_j|^2$ is the intensity of the respective propagating wave, $\mu = \partial^2 k/\partial\omega^2$ is the linear dispersion parameter, $\beta = n_2 k/n$ is the nonlinear parameter, n is the linear refractive index at the frequency ω, v_g is the linear group velocity, n_2 is the nonlinear refractive-index coefficient, and k is the wave number in the medium. The coefficient 2 on the right-hand side of Eq. (2) reflects light-induced nonreciprocity.[12] Losses due to absorption are not included in Eq. (2), since it can be shown that when the losses are small, they do not critically affect the phenomena related to instability and may result in only a slight change in the threshold intensity. However, the losses can become important for amplification with strongly subthreshold pumping, which is discussed in Section 6. The problem of temporal instability of cw propagation for certain signs of dispersion and nonlinearity is isomorphic to the problem of cross-induced self-focusing bistability[13] and spatial instability of plane counterpropagating waves in a nonlinear medium,[14] since the latter problem can be described by Eq. (2) in which the term with $\partial^2 E/\partial t^2$ is replaced by $\partial^2 E/\partial x^2$, where x is a coordinate in the transverse plane (i.e., spatial dispersion).

The steady solution for Eq. (2) is

$$E_{j0}(z) = \sqrt{I_{j0}}\exp\{i\beta(I_{j0} + 2I_{(3-j)0})(-1)^j[(j-1)L - z]\} \qquad j = 1,2, \tag{3}$$

where L is the length of the nonlinear medium and I_{10} and I_{20} are the intensities of the forward and backward propagating beams, respectively. There is no exchange of energy between the two beams in the *steady state*[2,3]; i.e., $|E_1|^2 = I_1 = I_{10}$ and $|E_2|^2 = I_2 = I_{20}$. By virtue of eigenpolarization, the electric fields E_1 and E_2 remain linearly polarized inside the nonlinear medium.

3. LINEAR STABILITY ANALYSIS

To analyze the small-perturbation stability of the steady state, we represent both waves in the system as slightly perturbed steady state in the form

$$E_j = E_{j0}(\xi)[1 + a_{1,j}\exp(\lambda\tau + \gamma\xi) + a_{2,j}{}^*\exp(\lambda^*\tau + \gamma^*\xi)] \qquad j = 1,2, \tag{4}$$

where $a_{1,j}$ and $a_{2,j}$ are some (small) constants, $\tau = tv_g/L$ is the normalized time, and $\xi = z/L$ is the normalized distance of propagation.

Both parameters λ and γ should be found based on boundary conditions (see below). However, the relation between them (i.e., dispersion relation) does not depend on boundary conditions and can be found straightforwardly. Indeed, substituting Eq. (4) into Eq. (2) and linearizing the latter equation with respect to small perturbations, we arrive at a system of four linear homogeneous algebraic equations for the amplitudes $a_{k,j}$:

$$\gamma a_{k,j} = i(-1)^{k+j}\{a_{k,j}[p_j - i(-1)^k\lambda - d\lambda^2] + p_j a_{3-k,j} + 2p_{3-j}(a_{1,3-j} + a_{2,3-j})\} \qquad j,k = 1,2, \tag{5}$$

where

$$p_j = \beta I_{j0}L, \qquad d = \mu v_g{}^2/2L.$$

Here the p_j's are the normalized pumping intensities of the two beams (note that p_j can have a negative sign depending on the nonlinearity β) and d is the normalized dispersion. For the system (5) to have a nontrivial solution, its determinant should be equal to zero, which results in the dispersion relation

$$\gamma^4 - 2\lambda^2[d(p_1 + p_2) + 1 - \lambda^2 d^2]\gamma^2 + \lambda^3 d(p_1 - p_2)\gamma + \lambda^4[1 + \lambda^2 d^2(\lambda^2 d^2 + 2) - 2d(1 + \lambda^2 d^2)(p_1 + p_2) - 12d^2 p_1 p_2] = 0. \tag{6}$$

At this point we further simplify our calculation, by assuming that both of the counterpropagating waves have equal intensities, i.e., $p_1 = p_2 = p$, and express all eigenvalues γ_j for each fixed λ as

$$\gamma_j = \gamma_{j+2} = \lambda[1 - (d\lambda)^2 + 2dp - (-1)^j 2x]^{1/2} \qquad j = 1,2, \tag{7}$$

where $x = [4(dp)^2 + 2dp - (d\lambda)^2]^{1/2}$. The elements of the corresponding eigenvector $\bar{v}_j$ are found from

$$v_{j,k} = \begin{cases} -\dfrac{2dp(\lambda - (-1)^{(k-1)/2}id\lambda^2 - \gamma_j)}{1 - (-1)^j x - \gamma_j\lambda^{-1}}, & k = 1,3, \\ & j = 1\text{–}4 \\ id\lambda^2 + (-1)^{k/2}\lambda - \gamma_j, & k = 2,4, \\ & j = 1\text{–}4 \end{cases} \tag{8}$$

where $v_{j,k}$ is the kth element in the eigenvector $\bar{v}_j$. It is obvious that the general form of perturbation for each fixed temporal eigenvalue λ must include all four spatial eigenvalues; i.e.,

$$E_j = E_{j0}(\xi)[1 + A_{1j}(\xi)\exp(\lambda\tau) + A_{2j}{}^*(\xi)\exp(\lambda^*\tau)] \qquad j = 1,2, \tag{9}$$

where

$$Ak,j(\xi) = \sum_{m=1}^{4} c_m v_{m,2(k-1)+j}\exp(\gamma_m\xi) \tag{10}$$

is the perturbation amplitude for $j = 1,2$ and $k = 1,2$ and the c_m's are constant coefficients to be determined by the boundary conditions for $m = 1$–4.

Since intensities of the forward pumping beam at the boundary $\xi = 0$ and the backward pumping beam at the

boundary $\xi = 1$ are determined by the respective incident (pumping) waves and therefore remain constant, the perturbation amplitudes $A_{k,j}$ *for* $k = 1, 2$ and $j = 1, 2$ must vanish, i.e., satisfy the boundary conditions

$$A_{1,1}(\xi = 0) = A_{1,2}(\xi = 1) = A_{2,1}(\xi = 0) = A_{2,2}(\xi = 1) = 0. \tag{11}$$

Four homogeneous algebraic equations result when Eq. (11) is substituted into Eq. (10). For a nontrivial solution of this set of equations to exist, the following condition must be satisfied:

$$D(\lambda, p, d) \equiv [H_{21}(\gamma_2) + H_{11}(\gamma_1)][H_{12}(\gamma_2) + H_{22}(\gamma_1)] + [J_1(\gamma_1) + J_2(\gamma_2)]^2 = 0, \tag{12}$$

where

$$H_{mn}(\gamma_j) = \frac{(\cosh \gamma_j)[\lambda x + i(-1)^m(d\lambda^2 - p)]}{2x\lambda} - (-1)^n(\sinh \gamma_j)(2\gamma_j x)^{-1} \times \{x[i(d\lambda^2 - p) + (-1)^n\lambda] + i(-1)^m[id\lambda + (-1)^n]d\lambda^2 - i(-1)^m p \times [2id\lambda + (-1)^n(1 + 4dp)]\}$$

and

$$J_j(\gamma_j) = i(p/2x)\{\gamma_j^{-1}(-1)^j(\sinh \gamma_j)[(-1)^{j+1}x + 4dp + 1] - (-1)^j\lambda^{-1}(\cosh \gamma_j)\}, \qquad m, n, j = 1, 2.$$

4. BOUNDARY OF INSTABILITY

The boundary separating the stable and unstable regions is found by setting $\mathrm{Re}(\lambda) = 0$ in Eq. (12). There are multiple solutions for this problem, each of which can be expressed, e.g., as threshold pumping intensity $p = (p_{cr})_{mode}$ [and respective normalized frequency $\Delta\Omega = \mathrm{Im}(\lambda)$] for a given dispersion d. Each of these solutions corresponds essentially to one of the light-induced longitudinal modes. The ultimate (encompassing) boundary of instability is associated with solutions having the lowest normalized threshold intensity $|p_{cr}|$ among these individual modes at a given dispersion d.

The numerical results of solving Eq. (12) are depicted in Fig. 2, which shows the normalized threshold intensity p_{cr} (>0) versus normalized dispersion d in a semilog plot. The solid curve is the ultimate (encompassing) boundary of instability. Above this boundary there are numerous solutions corresponding to various unstable modes of oscillation. As the dispersion decreases, the boundaries for individual modes are too closely packed to be shown in Fig. 2. These individual boundaries correspond to the longitudinal modes in a light-induced, distributed-feedback resonator. Only a few of these solutions and the boundary encompassing all the unstable solutions (i.e., the solid curve) are shown in Fig. 2.

The mode with the lowest frequency, which corresponds to the first dashed curve at the right in Fig. 2, has normalized oscillation frequency $\Delta\Omega \simeq 3\pi/2$ (numerically determined to be $\simeq 4.6$), whereas the first adjacent mode (with higher frequency) has $\Delta\Omega \simeq 5\pi/2$ ($\simeq 7.6$ numerically), and so on; i.e., each mode has its normalized oscillation frequency approximately π apart from the adjacent modes. The frequency $\Delta\Omega$ within each mode varies slowly with d; e.g., the deviation of $\Delta\Omega$ is less than 1% for an order-of-magnitude change in d. The same mode with lowest frequency (i.e., $\Delta\Omega \simeq 3\pi/2$) has the absolute minimum of the normalized critical pumping intensity $p_{cr} = p_m$ at $|d| = d_m$ (see Fig. 2), where

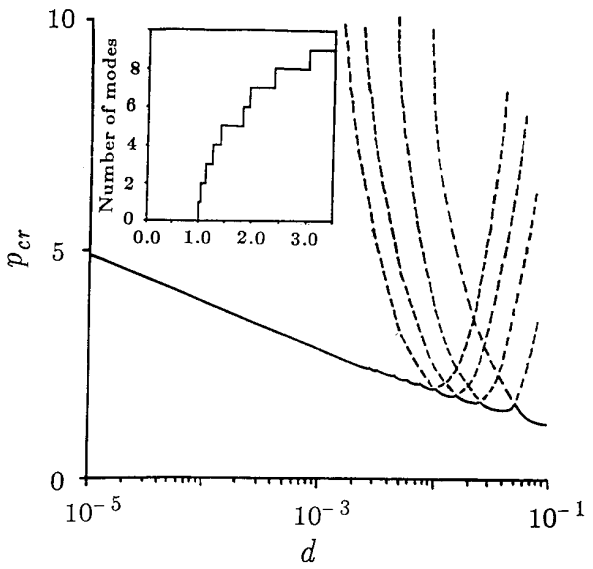

Fig. 2. Normalized threshold intensity p_{cr} versus normalized dispersion d. The solid curve is the boundary of instability above which the system is unstable. The dashed curves indicate boundaries of instability of individual modes. Inset: number of unstable modes versus $|p|/p_{cr}$, where p is the normalized driving intensity for normalized dispersion $|d| = 0.01$.

$$p_m = 1.2 \quad \text{and} \quad d_m = 0.095. \tag{13}$$

For $|d| > d_m$, p_{cr} increases rapidly, and only the lowest-frequency mode ($\Delta\Omega \simeq 3\pi/2$) determines the ultimate boundary of instability. Such a large dispersion parameter ($|d| = d_m$), even for a short medium length $L \lesssim 1$ m, corresponds to the physical dispersion $|\mu| \simeq 2 \times 10^{-18}$, which is at least several orders of magnitude higher than that of any real material (see the fiber example in Section 5). Therefore, for most of the realistic situations, one should expect $|d| \ll d_m \simeq 0.1$, so when the pumping even slightly exceeds the threshold of instability, the number of excited unstable modes becomes large.

Yet, since it is instructive to see how the number of modes increases as the pumping intensity exceeds the threshold of instability, we consider a dispersion parameter close to $|d| = d_m$; otherwise ($|d| \ll d_m$) the modes are too closely packed. In the inset in Fig. 2, the number of unstable modes is plotted against $|p|/p_{cr}$, where $p_{cr} = 1.98$ is the threshold intensity for the case $|d| = 0.01$ ($\simeq d_m/10$). One can see that when the pumping is only slightly above the threshold, only one mode becomes unstable, then two, and so on. When the number of modes is greater than 1, they compete with each other, and some of them can become dominant while others fade out (see the more detailed discussion in Section 5).

The (encompassing) threshold intensity increases as dispersion decreases; our numerical calculations show that for sufficiently small $|d|(\ll d_m)$, this dependence can be best described by the surprisingly simple relationship

$$p_{cr} = -\mathrm{sgn}(pd)\,|\log_\eta |d||, \tag{14}$$

where η is numerically determined to be $10.0 \pm 1\%$ and $\mathrm{sgn}(pd)$ is the sign of pd.

To gain physical insight into this dependence resulting from the complicated Eq. (12), we simplify Eq. (12) by assuming that the parameters $|d|$ and $|dp|$ are small and, therefore, that $|x|$ is small too: $x \simeq [2dp - (d\lambda)^2]1/2$ (and hence $\gamma_j \simeq \lambda[1 + (-1)^{j+1}x]$ when x is real and $\gamma_j \simeq \lambda \times [(-1)^{j+1} + x]$ when x is imaginary for $j = 1, 2$). After making the substitution $\lambda = i\Delta\Omega$, we obtain an approximate condition of instability in a simple form:

$$\cos(2\Delta\Omega) = -8[dp\,\sin(x\Delta\Omega)\cos(\Delta\Omega)/x]^2, \tag{15a}$$

$$\sin(2\Delta\Omega) = 4(dp)^2\,\sin(2x\Delta\Omega)/x. \tag{15b}$$

From Eq. (15b), it is obvious that $\Delta\Omega$ must have a value slightly less than an integer multiple of $\pi/2$. As the right-hand side of Eq. (15a) is negative, we deduce that $\Delta\Omega = (n + 1/2)\pi - h(p,d)$ where n is a nonnegative integer and $h(p,d)$ is a function of p and d, $0 \le h \ll 1$, which indicates a perfectly expected formation of the light-induced resonator with mode spacing $\simeq c/2L$. In order that nontrivial solutions from Eq. (15a) and (15b) may be obtained, x must be imaginary, which implies that $dp < 0$. Setting $\Delta\Omega \simeq (-p/d)^{1/2}$, which is the frequency of the excited mode with the lowest threshold for a particular d, we immediately obtain an approximate analytical relation between p_{cr} and d that is exactly the same as Eq. (14) except for a crude estimate of $\eta \sim e^{3/2}$.

As we see, since the product pd must be negative to initiate instability (i.e., to have $p_{cr} > 0$), the signs of nonlinearity n_2 and dispersion μ must be opposite, which coincides with the necessary condition for formation of a soliton and for spatial instability in single-wave propagation. Under such a condition, the medium should exhibit either anomalous dispersion with a self-focusing type of nonlinearity or normal dispersion with a self-defocusing type of nonlinearity. In terms of the original parameters of the problem, Eq. (14) can be rewritten as

$$I_{cr} = -\frac{\mathrm{sgn}(\mu)}{n_2 kL}\left|\log_\eta\left(\frac{2L}{|\mu|v_g^{\,2}}\right)\right|, \tag{16}$$

where $I_{cr} = p_{cr}/L|\beta|$ is the threshold intensity ($|E|^2$) of pumping. This formula shows, in particular, that I_{cr} decreases as the length L of the medium increases.

5. TEMPORAL DYNAMICS

To explore the full dynamical behavior in stable and unstable regions shown in Fig. 2, we numerically integrate Eq. (2) with the method of lines. We divide the problem into small time intervals within each of which Eq. (2) is discretized into a set of first-order ordinary equations at each temporal collocation point with boundary conditions at $\xi = 0$ and $\xi = 1$. The unknown solution is expanded in terms of Chebyshev polynomials temporally and in terms of piecewise continuous basis functions spatially. As a result, we must solve a large system of nonlinear algebraic equations for the coefficients at each time step; this task was carried out by a supercomputer.

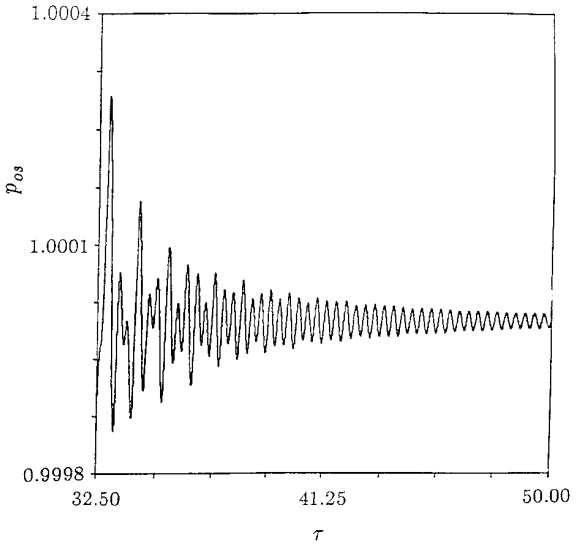

Fig. 3. Normalized intensity p_{os} of oscillations versus normalized time τ for driving intensities $|p/p_{cr}| = 0.96$ (under-threshold pumping; damped oscillations and fixed normalized dispersion $|d| = 0.01$ with $p_{cr} = 1.98$).

We brought the system to the desired steady-state output fields by slowly ramping the input fields in time and maintained them at this level with the dispersion fixed at $|d| = 0.01$ [as previously, we chose this unrealistically large dispersion parameter for the sake of illustrating the appearance of new unstable modes; see also the discussion following Eq. (14)]. Figure 3 shows that within the stable region, i.e., $|p| = 1.9 < p_{cr} = 1.98$ (under-threshold pumping with $|p/p_{cr}| = 0.96$), the initial perturbation is decaying as the normalized time $\tau = tv_g/L$ increases. In the unstable region (i.e., $|p| > p_{cr}$), we let the instability be excited by the computer noise. The slow increase of intensity of oscillations, p_{os}, with τ when the intensity is slightly greater than the threshold ($|p/p_{cr}| = 1.02$) is shown in Fig. 4. At such a pumping intensity, only one mode is unstable (see the inset of Fig. 2) and eventually develops into periodic self-sustained oscillations with a stable amplitude. When the value of $|p/p_{cr}|$ is further increased to 1.28, the instability and resulting self-sustained oscillations develop much faster, as is shown in Fig. 5. In this case three modes satisfy the excitation condition (see the inset of Fig. 2); as the oscillations develop in time, the second subharmonic is excited, which later evolves into aperiodic oscillations with randomly modulated amplitude and phase that indicate onset of chaos. We expect this behavior to develop further into strongly pronounced chaos when the pumping intensity is significantly higher than the threshold, and therefore more unstable modes with different eigenfrequencies will survive and compete.

In order to estimate the threshold intensity for instability, we consider an example of a 1-km-long single-mode fiber with Ge-doped silica core at wavelength 1.55 μm

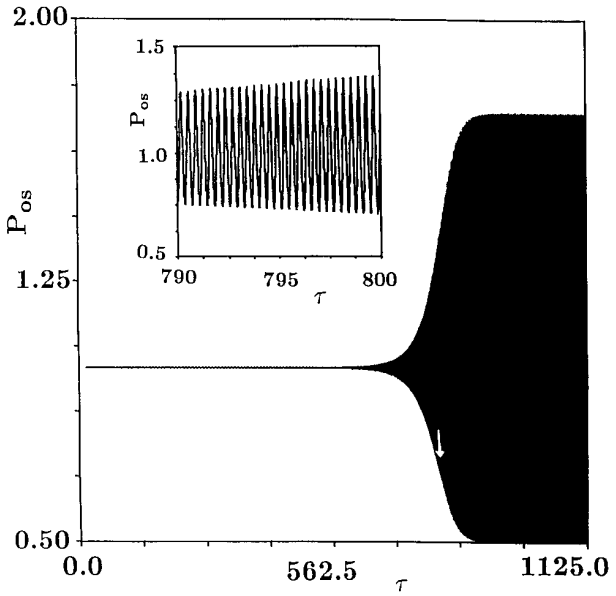

Fig. 4. Normalized intensity p_{os} of oscillations versus normalized time τ for driving intensities $|p/p_{cr}| = 1.02$ (single-mode oscillations; fixed normalized dispersion $|d| = 0.01$ excitation with $p_{cr} = 1.98$); the inset depicts the enlargement of the region indicated by the arrow and demonstrates the single-mode nature of the excitation. The frequency of oscillations is $\approx 17.2\, v_g L^{-1}$.

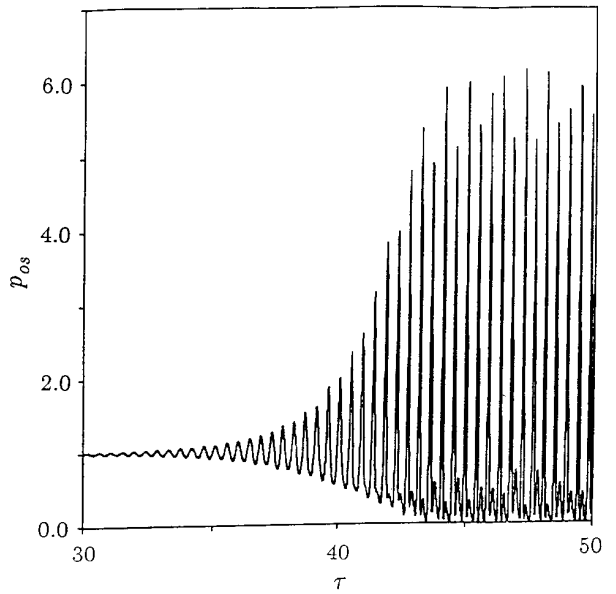

Fig. 5. Normalized intensity p_{os} of oscillations versus normalized time τ for driving intensities $|p/p_{cr}| = 1.25$ (three unstable modes are engaged for $p_{cr} = 1.98$); the excitation shows the formation of a subharmonic and the onset of chaos. The initial frequency of oscillations is slightly less than that in Fig. 4.

with group-velocity dispersion $D(k) = 6.5 \times 10^{-3}$ [note that $\mu = -D(k)/kc^2$; the corresponding $d = -8.02 \times 10^{-13}$], refractive index $n = 1.44$, and $n_2 = 3.2 \times 10^{-16}$ cm^2/W,[15] in the lossless approximation. We find the threshold intensity I_{cr} [Eq. (14)] for such a fiber to be 9.3 MW/cm^2, which is below the damage threshold 10^{10} W/cm^2 for fused silica.[16] A crude estimate shows that the losses existing in the real fiber [~0.5 dB/km (Ref. 15)] would require only approximately two times higher threshold intensity. If we use the SF-59 glass with $n_2 = 7 \times 10^{-15}$ cm^2/W (Ref. 17) at wavelength 1.06 μm, and assume the n_2 at wavelength 1.55 μm is of the same order as that at 1.06 μm and that dispersion is roughly the same as for plain glass, the critical intensity is reduced to ~425 kW/cm^2 for the same length. (One can trade in the pumping intensity for a shorter fiber length if one keeps the intensity at the threshold for Ge-doped silica fiber.) It is worth noting that for the same example (Ge-doped silica fiber) the relaxation-related instability[6] is prohibited. Indeed, we found that the threshold of instability for the relaxation-related mechanism would require the threshold intensity of $\sim 7.4 \times 10^{13}$ W/cm^2 (i.e., much higher than the damage threshold), which is due to the intrinsically fast response of nonlinearity in glass (<100 fsec).[18]

A few other facets of the problem should be briefly mentioned. The current analysis is applicable to a quasi-cw regime in which the pulse lengths cover the whole fiber; however, a short fiber length can relax the requirement on the pumping pulse durations. Since our goal here is to demonstrate the role of dispersion as a possible mechanism of temporal instability in nonlinear counterpropagating waves, we did not consider other competing effects, such as stimulated Raman and Brillouin scattering, directly in our calculation. The first unstable mode excited in the Ge-doped case owing to dispersion occurs at a frequency of 1.2 THz shifted from the pumping frequency. A rough estimate shows that the threshold intensity for the stimulated Raman scattering at this frequency is ~100 MW/cm^2 (i.e., above the threshold of dispersion-related instability, which is ~9.3 MW/cm^2). This indicates that even if the stimulated Raman scattering is excited (at much higher frequency, ~13 THz shifted from the pumping frequency[16]), it may coexist with the instability under consideration (or even be suppressed by it). The stimulated Brillouin scattering may be suppressed by using a driving signal with a sufficiently broad spectral line[19]; it is clear nevertheless that the competition of all these three processes presents an interesting subject for further investigation.

6. AMPLIFICATION

So far we have considered above-threshold pumping by two counterpropagating laser beams, which have the same frequencies and intensities, in a dispersive Kerr nonlinear medium. In this section we demonstrate that the system may exhibit large (theoretically unlimited) small-signal amplification when the intensities of two pumping beams are *below* the threshold. This amplification can have broad bandwidth (even when the pumping intensity is much smaller than the threshold intensity), with the frequency of the maximal gain shifted significantly away from the pumping.[20]

Similar to temporal instability, amplification in this system can be explained in terms of positive distributed feedback from a light-induced, distributed-feedback resonator, attributed to the Kerr nonlinear index grating (produced by two strong pumping laser beams) in the presence of linear dispersion. This feedback occurs because the weak beams with both signal frequency $\Omega + \delta\Omega$ and conjugate frequency $\Omega - \delta\Omega$ propagate with a phase speed

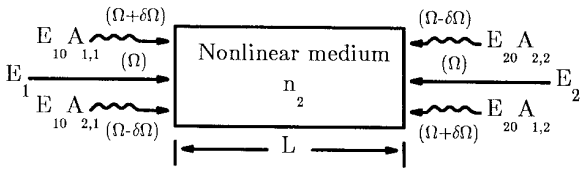

Fig. 6. Pump-probe configuration for amplification measurement, where E_1 and E_2 are the pumping waves and $E_{10}A_{1,1}$ is the input probe wave, with $E_{10}A_{2,1}$, $E_{20}A_{1,2}$ and $E_{20}A_{2,2}$ generated as a result of the wave mixing process.

differing (owing to dispersion) from that of pumping waves with normalized frequency $\Omega = \omega L/v_g$. The difference between the phase speeds triggers the exponentially increasing energy exchange between weak and strong beams at the nonlinear index grating, this exchange being prohibited in nondispersive media. When the probe frequency approaches one of the longitudinal modes of the light-induced distributed resonator, and the pumping intensity approaches the threshold of instability, the resonant amplification for small signals increases theoretically to infinity.

To find the gain spectrum of this system, we inject a weak probe beam into the nonlinear medium and scan the beam frequency. In Fig. 6 we show a new configuration with two pump beams and four weak beams. Suppose that the probe beam ($E_{10}A_{1,1}$) has frequency $\Omega + \delta\Omega$, i.e., its frequency is deviated by $+\delta\Omega$ from that of the pump beams with normalized frequency Ω; then we expect a phase-conjugate signal ($E_{20}A_{2,2}$) to be reflected back with frequency $\Omega - \delta\Omega$. These two beams are referred to as direct-coupled waves.[22] The remaining two weak beams are referred to as cross-coupled forward ($E_{10}A_{2,1}$) and backward ($E_{20}A_{1,2}$) waves with frequencies equal to $\Omega - \delta\Omega$ and $\Omega + \delta\Omega$, respectively. Since we consider a collinear geometry, the effect of the cross-coupled waves cannot be neglected.[22]

Since the only differences between perturbation in Section 2 and the four signal waves here are that the boundary condition for one of the signal waves (specifically, for a probe wave) is nonzero, and since the detuning frequency is set by the probe wave, we can treat $A_{1,1}$, $A_{2,1}$, $A_{1,2}$, and $A_{2,2}$ here by using the same procedure outlined in Section 2. Therefore we look for a solution in the form of Eq. (10) with the boundary conditions

$$A_{1,1}(\xi = 0) = C = \text{const.},$$

$$A_{2,1}(\xi = 0) = A_{1,2}(\xi = 1) = A_{2,2}(\xi = 1) = 0.$$

The numerical results of our calculations are shown in Figs. 7–9. First, we again deliberately choose an artificially large value of the normalized dispersion parameter, namely, $d = 0.01$ (which is significantly higher than what may be expected in a real experiment; see Section 4), in Figs. 7 and 8 in order to demonstrate the spatial and spectral features of these waves, in particular, the resonances associated with the eigenmodes. Then we consider some realistic examples; see the text below and Fig. 9.

In Figs. 7(a) and 7(b) we depict the spatial variation of the normalized intensities $Q_{1,1} = |A_{1,1}(\xi)/A_{1,1}(0)|^2$, $Q_{2,1} = |A_{2,1}(\xi)/A_{1,1}(0)|^2$, $Q_{1,2} = |A_{1,2}(\xi)/A_{1,1}(0)|^2$, and $Q_{2,2} = |A_{2,2}(\xi)/A_{1,1}(0)|^2$ for $|d| = 0.01$. These plots correspond to the pumping intensity $|p| = 1.9$, which is close to the threshold of instability (i.e., $|p/p_{cr}| = 0.96$), and to the normalized detuning frequency $\delta\Omega = 14$, which is close to the frequency of one of the resonant modes $\delta\Omega_R = 4.5\pi$. All the intensities oscillate in space at twice the normalized detuning frequency and clearly exhibit the exponential growth. Figure 7(a) shows that the probe beam $A_{1,1}$ leads the forward cross-coupled wave $A_{2,1}$ at the boundary ($\xi = 0$), and eventually both reach the other end of the

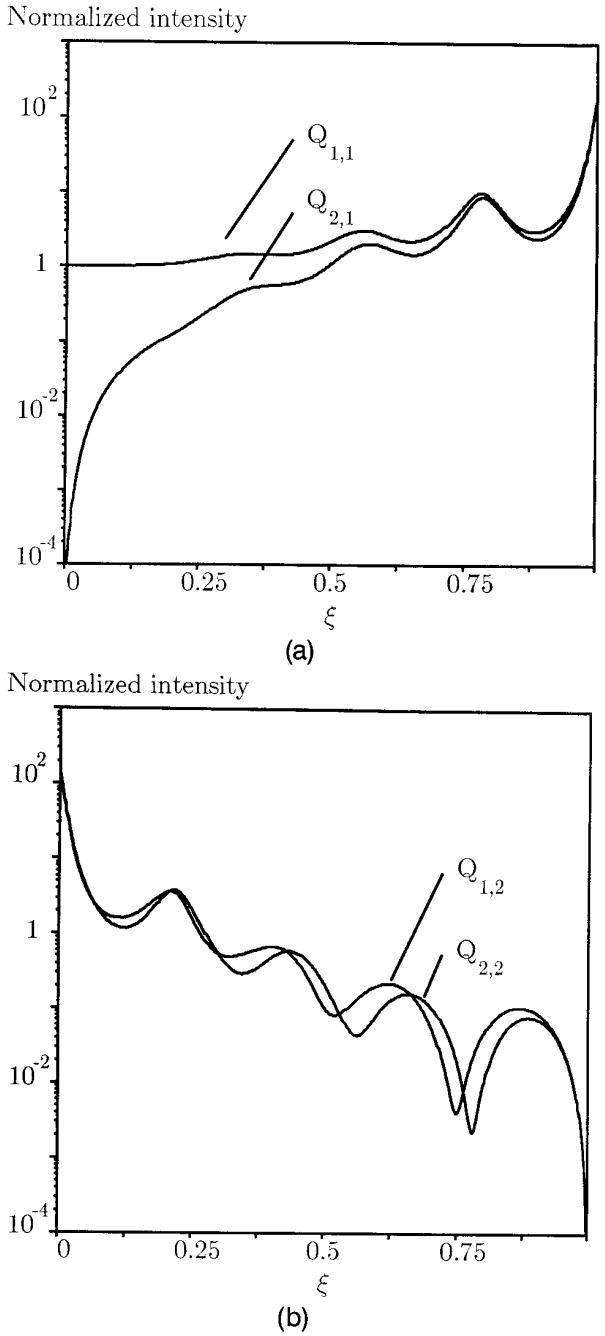

Fig. 7. Behavior of normalized intensities (a) $Q_{1,1}$ of the probe wave and $Q_{2,1}$ of the forward propagating cross-coupled wave and (b) $Q_{2,2}$ of the phase-conjugated wave and $Q_{1,2}$ of the backward traveling cross-coupled wave as functions of the normalized propagation distance ξ when pumping intensity $|p| = 1.9$, normalized detuning frequency $\delta\Omega = 14$, normalized dispersion $|d| = 0.01$, and $p_{cr} = 1.98$.

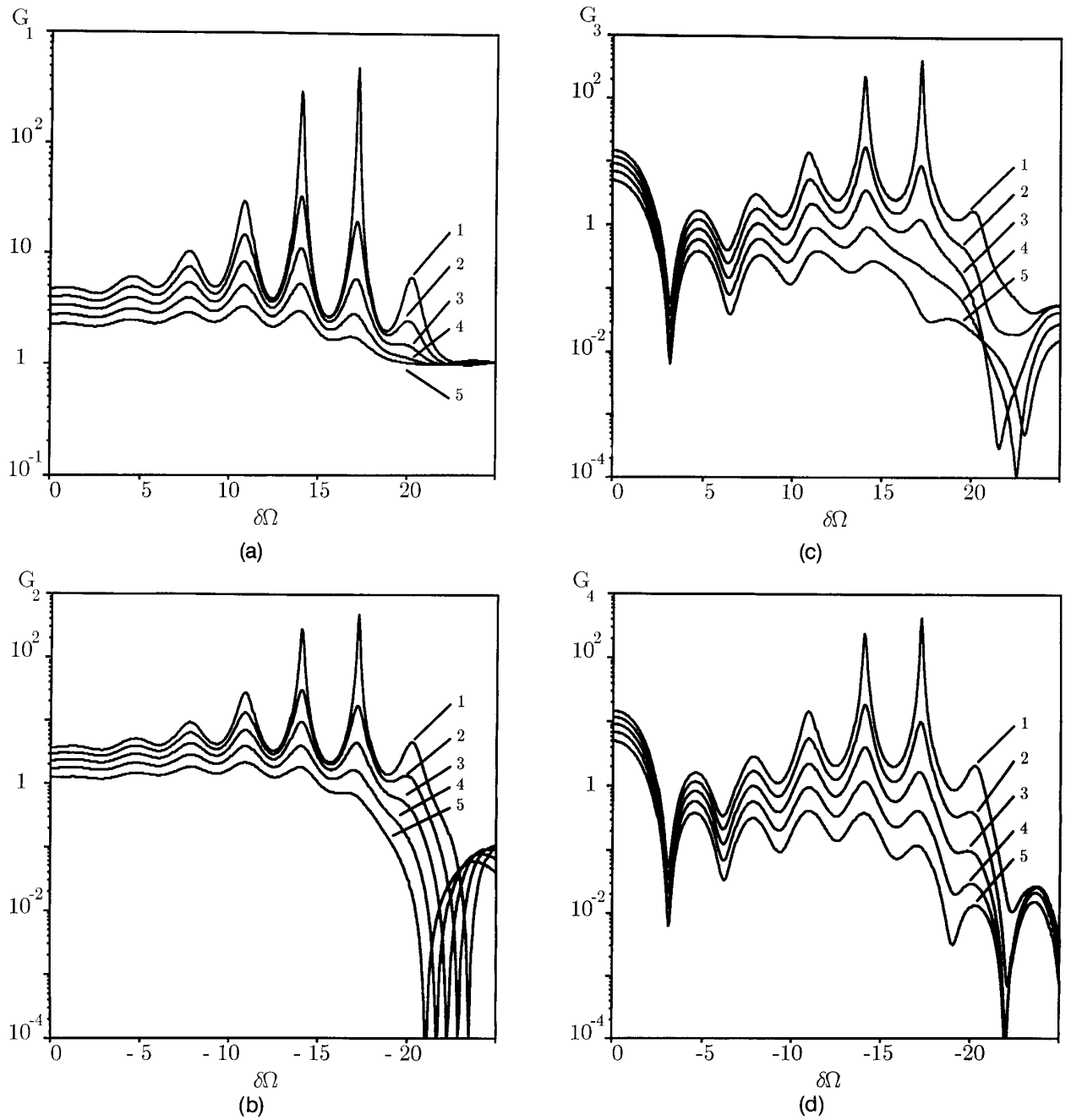

Fig. 8. (a) Amplification G_1 of the probe wave, and transformation coefficients (b) G_2 of the forward traveling cross-coupled wave, (c) G_3 of the backward traveling cross-coupled wave, and (d) G_4 of the phase-conjugated wave, each versus normalized frequency detuning $\delta\Omega$ when normalized dispersion $|d| = 0.01$ and $p_{cr} = 1.98$. Curves: $1-|p/p_{cr}| = 0.98$; $2-|p/p_{cr}| = 0.88$; $3-|p/p_{cr}| = 0.78$; $4-|p/p_{cr}| = 0.68$; and $5-|p/p_{cr}| = 0.58$.

medium at $\xi = 1$ with approximately the same intensities. A similar spatial behavior of the backward propagating conjugate wave $A_{2,2}$ and cross-coupled wave $A_{1,2}$ is shown in Fig. 7(b).

We define the intensity amplification G_1 for the probe wave $A_{1,1}$, and the transformation coefficients $G_k (k = 2, 3, 4)$ for the rest of the signal waves, as

$$G_1 = |A_{1,1}(\xi = 1)/A_{1,1}(\xi = 0)|^2,$$

$$G_2 = |A_{2,1}(\xi = 1)/A_{1,1}(\xi = 0)|^2,$$

$$G_3 = |A_{1,2}(\xi = 0)/A_{1,1}(\xi = 0)|^2,$$

$$G_4 = |A_{2,2}(\xi = 0)/A_{1,1}(\xi = 0)|^2.$$

The variation of G_1, G_2, G_3, and G_4 with normalized frequency detuning $\delta\Omega$ is depicted in Figs. 8(a)–8(d) with dispersion $|d| = 0.01$, for various pumping powers (below threshold). Figures 8(a)–8(d) indicate that the bandwidth and the distribution are essentially the same for all four waves. Their bandwidth for the case when pumping in-

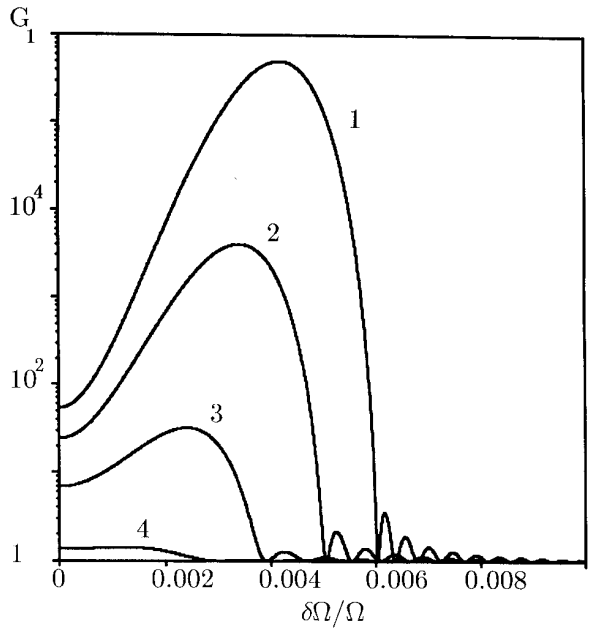

Fig. 9. Amplification G_1 of the probe wave versus frequency-modulation index $\delta\Omega/\Omega$ for the case of a 1-km-long Ge-doped silica fiber. Curves: 1—60% of instability threshold p_{cr} (120 times the amplification threshold I_{amp}); 2—40% of p_{cr} (80 × I_{amp}); 3—20% of p_{cr} (40 × I_{amp}); and 4—5% of p_{cr} (10 × of I_{amp}).

tensity is equal to 98% of the threshold of instability is approximately $\delta\Omega = 22$.

In Figs. 8(a)–8(d), there are several peaks, each corresponding to the possible eigenmodes that can be excited at the onset of instability (see Fig. 2). The two outstanding peaks at $\delta\Omega \simeq 14$ and $\delta\Omega \simeq 17$ are the ones excited first under an unstable regime. As noted in Section 2, the spacing between peaks (or modes) is approximately π, which is the reciprocal of round-trip time $(c/2L)$ in the medium, the same as, e.g., the mode spacing in a distributed-feedback laser.[23]

On comparison of the spectra of backward and forward propagating waves, one notices that G_3 and G_4 for the backward propagating waves in Figs. 8(c) and 8(d) resemble G_2 in Fig. 8(b), except that there is a peak near $\delta\Omega = 0$. This additional peak corresponds to the conventional four-wave mixing gain in a system without linear dispersion.[21] Actually, this conventional gain also appears in G_1 and G_2 near $\delta\Omega = 0$, at which the gain would be 1 for G_1 and 0 for G_2 if there were no four-wave mixing process. This conventional gain is approximately an order of magnitude lower than that of the dispersion-related amplification for G_3 and G_4 and is even lower relative to the dispersion-related amplification for G_1 and G_2.

Pumping slightly below the threshold has the definite advantage of attaining higher small-signal gain (theoretically approaching infinity). However, one cannot pump too close to the threshold of instability, since an amplitude noise introduced by the laser may trigger the system into instability. Another disadvantage of near-threshold pumping in the case when $|d|$ is close to d_m is the variation of amplification over a narrow bandwidth owing to the nonlinear resonant modes. In the example above we deliberately used an overly large parameter $d = \mu v_g^2/2L$—that is, for fixed disperison μ we chose a short interaction length L and an excessively strong nonlinearity (since $p = n_2 kLI$)—in order to decrease significantly the number of eigenmodes engaged and thus demonstrate the resonance.

In any practical situation, however, the parameter $|d|$ is small, kL is large, and the resulting amplification may be large (while the resonant peak structure disappears) even when the pumping is substantially below the threshold. Indeed, let us consider again the same example discussed in Section 5, i.e., the 1-km-long silica core Ge-doped optical fiber. The gain spectrum for this system is demonstrated in Fig. 9, in which the amplification G_1 of the probe wave is shown versus frequency detuning with pumping at 60%, 40%, 20%, and 5% of the threshold intensity $I_{cr} = 9.3$ MW/cm^2. One can see that even when the pumping is well below the threshold of instability, the bandwidth and the amplification are still appreciable. For instance, in the case of pumping at 20% of the threshold of instability, the gain is $\simeq 20$ and the bandwidth is $\simeq 2.5 \times 10^6$ (7.4×10^{11} Hz or 0.4% of the pumping frequency). Unlike the artificial case in Figs. 8(a)–8(d) with large dispersion d and near-threshold pumping, the gain spectra in Fig. 9 are smooth (no pronounced resonances are present).

So far we have discussed the gain spectrum shown in Figs. 8 and 9, which are obtained by numerical calculations. It is instructive to have an analytical approximation for the gain spectrum in order to gain further insight. It was found by us that for $d \ll d_m$, the gain G_1 can be represented approximately as

$$G_1 \simeq \begin{cases} 1 + p^2 + 2(1 + p^2/3)|dp|\,\delta\Omega^2 & \text{for } \delta\Omega \ll (\delta\Omega)_0 = (8|pd|)^{-1/2}\ln(1 + p^2) \\ \dfrac{\exp\{2\delta\Omega[2|dp| - (d\delta\Omega)^2]^{1/2}\}}{|D(\lambda = i\delta\Omega, p, d)|^2} & \text{for } \delta\Omega > (\delta\Omega)_0 \end{cases}, \quad (17)$$

where D is the determinant defining the threshold of instability in Eq. (12). Formula (17) correctly predicts that the gain slowly rises from $p^2 + 1$, its value at $\delta\Omega = 0$, when $\delta\Omega < (\delta\Omega)_0$. This portion of the gain spectrum for $\delta\Omega \ll (\delta\Omega)_0$ corresponds to the contribution from dispersionless four-wave mixing. Beyond $(\delta\Omega)_0$ the variation of gain obeys $\sim\exp\{2\delta\Omega[2|dp| - (d\delta\Omega)^2]^{1/2}\}$ when pumping power $|p|$ is substantially below p_{cr}. This part of the gain is caused solely by a dispersion-related process. The determinant D, which is equal to 1 in most conditions (especially in the realistic situation when $|d| \ll d_m$) except at near-threshold pumping ($p_{cr} - |p| \ll p_{cr}$), is responsible for the resonant modes and the instability. Since if $D = 0$ (at least at one possible frequency, $\delta\Omega = \Delta\Omega$) at $|p| = p_{cr}(d)$, $G_1 \to \infty$ as $|p| \to p_{cr}$. (Naturally, if $G = \infty$ at least at one frequency, the entire system becomes unstable, which therefore would exclude steady-state amplification for any other frequencies.) The value of gain in formula (17) deviates from the numerical results by at most a factor of 2–4. The maximum deviation usually occurs at the peak gain. For instance, when pumping is 20% of the instability threshold in Fig. 9, formula (17) in-

dicates a peak gain of 66, whereas the numerical calculation gives 20.

From formula (17) one can note that a nonzero amplification (or $G_1 > 0$) can be obtained for any pumping intensity; however, for each fixed intensity $|p|$, the frequency detuning should be smaller than a certain cutoff frequency $(\delta\Omega)_{cr}$:

$$|\delta| \leq (\delta\Omega)_{cr} \simeq (2|p/d|)^{1/2}. \tag{18}$$

Therefore, a rough estimate of the amplification bandwidth is given by $(\delta\Omega)_{cr}$ [formula (18)], which is valid for arbitrary pumping ($|p| < p_{cr}$). The maximum bandwidth $(\delta\Omega)_{max}$ for a fixed dispersioin d is attained when $|p| = p_{cr}$ [Eq. (14)]; i.e.,

$$(\delta\Omega)_{max} \simeq (2|\log_\eta|d|/d|)^{1/2}. \tag{19}$$

Formula (19) gives a good approximation for the maximum bandwidth even when the condition $d \ll d_m$ is not satisfied; for instance, in Figs. 8(a)–8(d) the maximum bandwidth $(\delta\Omega)_{max} \simeq 22$, whereas according to formula (19), $(\delta\Omega)_{max} = 20$. The location of the peak gain $(\delta\Omega)_{opt}$, i.e., the frequency of the mode with the lowest threshold of instability, can be approximately estimated as

$$(\delta\Omega)_{opt} = (\delta\Omega)_{cr}/\sqrt{2}. \tag{20}$$

The results from these approximate equations for frequency [formulas (18)–(20)] are qualitatively close to the exact values from numerical calculation shown in Fig. 9. For example, the gain spectrum for pumping at 20% of the threshold in Fig. 9 gives $(\delta\Omega)_{cr} \simeq 2.46 \times 10^6$ (0.4% of the pumping frequency) and $(\delta\Omega)_{opt} \simeq 1.53 \times 10^6$ (0.25% of the pumping frequency), whereas formulas (18) and (20) give $(\delta\Omega)_{cr} \simeq 1.74 \times 10^6$ (0.28% of the pumping frequency) and $(\delta\Omega)_{opt} \simeq 1.23 \times 10^6$ (3.7×10^{11} Hz or 0.2% of the pumping frequency), respectively. The results from these equations converge to the exact values as $|p|$ increases, e.g., both approximate and exact calculations indicate that $(\delta\Omega)_{cr} = 0.6\%$ of the pumping frequency when pumping is 60% of the threshold in Fig. 9.

The results above indicate that the nonlinear fiber with dispersion, pumped by counterpropagating waves, has great potential as an all-optical amplifier operating in a cw or quasi-cw regime, which may find applications in optical gyroscopes, optical fiber communications, etc. One possible limiting factor in amplification is the losses in the fiber, which have not been included in our calculation. To estimate the effect of losses in the optical fiber, we introduce a threshold intensity of amplification, I_{amp}, that satisfies the condition

$$\alpha L = \Gamma(I_{amp}), \tag{21}$$

where α is the loss coefficient and $\Gamma(I_{amp})$ is the growth rate at the amplification threshold in the lossless approximation (i.e., the gain must be equal to the loss at I_{amp}). Substituting formulas (17), (18), and (20) into Eq. (21), we obtain a remarkably simple expression for I_{amp} at $(\delta\Omega)_{opt}$:

$$I_{amp} = \alpha/2n_2k, \tag{22}$$

which does not depend on either length or dispersion. For the silica fiber considered in Section 5, $\alpha = 0.5$ dB/km = 0.12 km^{-1} (Ref. 15) and $n_2k = 1.3 \times 10^{-6}$ km^{-1} (Ref. 16). Hence the threshold of amplification is 46.2 kW/cm^2 (or 0.5% of the threshold of instability in the example, with $L = 1$ km and $\mu = 14$ psec/(nm-km). For a typical fiber with an effective area of 50 μm^2,[15,16] the threshold pumping power for amplification is 23 mW. This excellent performance is attributed to the low loss in the fiber.

Although our master equations (2)–(6) are valid for arbitrary intensities of both pumping beams, for our calculation beyond Eq. (6) we considered only equal pumping. Our preliminary estimates show that the amplification in this system is insensitive to a slight imbalance of pumping intensities. A large imbalance, on the other hand, is known to result in suppression of the nonreciprocal phase shift[12] and large gain in phase-conjugate reflectivity[24] and certainly may affect amplification and result in its suppression as one of the pumping intensities vanishes.

7. CONCLUSION

We showed that linear frequency dispersion, together with Kerr nonlinearity, can result in amplification and temporal instability of nonlinear counterpropagating waves. This suggests that regular linear dispersion can be a universal agent for amplification of perturbations and the resulting instability (and self-oscillations) in the nonlinear counterpropagating waves. As the pumping increases above a certain threshold, self-oscillations are excited; on further increase of pumping they evolve into subharmonics and chaos. With under-threshold pumping, large gain and broadband amplification are to be found. The mechanism of the entire phenomenon can be explained in terms of positive distributed feedback from the nonlinear index grating formed by the two laser beams. The feedback is attributed to the fact that small perturbations with different frequencies propagate with phase speeds different (owing to dispersion) from that of the fundamental wave, which gives rise to the energy exchange between two waves at the nonlinear index grating (such an exchange is prohibited in steady state and in the nondispersive medium). Our calculations show that the amplifiers based on the nonlinear optical fiber pumped by counterpropagating waves with relatively low power have great potential for various applications.

ACKNOWLEDGMENTS

This research was supported by the U.S. Air Force Office of Scientific Research; the numerical results were obtained using the Cray-XMP computer at the Pittsburgh Supercomputing Center.

REFERENCES AND NOTES

1. H. G. Winful and J. H. Marburger, Appl. Phys. Lett. **36,** 613 (1980).
2. A. E. Kaplan, Opt. Lett. **8,** 560 (1983).
3. A. E. Kaplan and C. T. Law, IEEE J. Quantum Electron. **21,** 1529 (1985).
4. A. L. Gaeta, R. W. Boyd, J. R. Ackerhalt, and P. W. Milonni, Phys. Rev. Lett. **58,** 2432 (1987); G. Khitrova, J. F. Valley, and H. M. Gibbs, Phys. Rev. Lett. **60,** 1126 (1988); D. J. Gauthier, M. S. Malcuit, and R. W. Boyd, Phys. Rev. Lett. **61,** 1827 (1988).

5. J. Yumoto and K. Otsuka, Phys. Rev. Lett. **54,** 1806 (1985); M. V. Tratnik and J. E. Sipe, Phys. Rev. A **35,** 2965 (1987).
6. I. Bar-Joseph and Y. Silberberg, Phys. Rev. A **36,** 1731 (1987); Y. Silberberg and I. Bar-Joseph, Phys. Rev. Lett. **48,** 1541 (1982); J. Opt. Soc. Am. B **1,** 662 (1984).
7. C. T. Law and A. E. Kaplan, Opt. Lett. **14,** 734 (1989).
8. S. A. Akhmanov, R. V. Khokhlov, and A. P. Sukhorukov, in *Laser Handbook,* F. T. Arecchi and E. O. Schulz-DuBois, eds. (North-Holland, Amsterdam, 1972).
9. V. E. Zakharov and A. B. Shabat, Sov. Phys. JETP **34,** 62 (1972); A. Hasegawa and F. Tappert, Appl. Phys. Lett. **23,** 142 (1973).
10. G. P. Agrawal, Phys. Rev. Lett. **59,** 880 (1987).
11. C. Pare, M. Piche, and P.-A. Belanger, J. Opt. Soc. Am. B **5,** 676 (1988).
12. A. E. Kaplan and P. Meystre, Opt. Lett. **6,** 590 (1981); Opt. Commun. **40,** 229 (1982); R. A. Bergh, H. C. Lefevre, and H. J. Shaw, Opt. Lett. **7,** 282 (1982); S. Ezekiel, J. L. Davis, and R. W. Hellwarth, Opt. Lett. **7,** 457 (1982).
13. J. E. Bjorkholm, P. W. Smith, W. J. Tomlinson, and A. E. Kaplan, Opt. Lett. **6,** 345 (1981); A. E. Kaplan, Opt. Lett. **6,** 360 (1981); I. C. Khoo, Appl. Phys. Lett. **41,** 909 (1982); K. Tai, H. M. Gibbs, N. Peyghambarian, and A. Mysyrowicz, Opt. Lett. **10,** 220 (1985).
14. W. J. Firth and C. Pare, Opt. Lett. **13,** 1096 (1988).
15. J. W. Fleming, J. Am. Ceram. Soc. **59,** 503 (1976); T. Li, IEEE Trans. Commun. **COM-26,** 946 (1978).
16. R. Hellwarth, J. Cherlow, and T. T. Yang, Phys. Rev. B **11,** 964 (1975); R. H. Stolen, in *Optical Fiber Telecommunications,* S. E. Miller and A. G. Chynoweth, eds. (Academic, New York, 1979), p. 125; R. G. Smith, Appl. Opt. **11,** 2489 (1972).
17. S. R. Friberg and P. W. Smith, IEEE J. Quantum Electron. **QE-23,** 2089 (1987).
18. I. Thomazeau, J. Etchepare, G. Grillon, and A. Migus, Opt. Lett. **10,** 223 (1985).
19. Decreased coherence may even slightly enhance the condition of instability, since the waves with frequencies slightly deviated from that of the pumping are amplified even below the threshold (see Section 6).
20. This shift of the frequency of maximal gain away from the pumping frequency is in contrast to the "conventional" phase conjugation[21] attributed to four-wave mixing in a nondispersive Kerr nonlinear medium.
21. D. M. Pepper and A. Yariv, in *Optical Phase Conjugation,* R. A. Fisher, ed. (Academic, New York, 1982), p. 24.
22. J. H. Marburger, in *Optical Phase Conjugation,* R. A. Fisher, ed. (Academic, New York, 1982), p. 99.
23. H. Kogelnik and C. V. Shank, J. Appl. Phys. **43,** 2327 (1972).
24. J. M. Marburger and J. F. Lam, Appl. Phys. Lett. **35,** 249 (1979).